Hindawi Publishing Corporation
ISRN Biomedical Imaging
Volume 2013, Article ID 473437, 10 pages
http://dx.doi.org/10.1155/2013/473437

Research Article

Automated Brain Tissue Classification by Multisignal Wavelet Decomposition and Independent Component Analysis

Sindhumol S.,[1] Anil Kumar,[2] and Kannan Balakrishnan[1]

[1] *Artificial Intelligence Lab, Department of Computer Applications, Cochin University of Science and Technology, Kochi 682022, India*
[2] *Institute of Radiology and Imaging Sciences, Indira Gandhi Co-Operative Hospital, Kochi, Kerala 682020, India*

Correspondence should be addressed to Sindhumol S.; sindhumol09@gmail.com

Received 4 February 2013; Accepted 26 March 2013

Academic Editors: W. Hall, I. Karanasiou, and G. Waiter

Multispectral analysis is a potential approach in simultaneous analysis of brain MRI sequences. However, conventional classification methods often fail to yield consistent accuracy in tissue classification and abnormality extraction. Feature extraction methods like Independent Component Analysis (ICA) have been effectively used in recent studies to improve the results. However, these methods were inefficient in identifying less frequently occurred features like small lesions. A new method, Multisignal Wavelet Independent Component Analysis (MW-ICA), is proposed in this work to resolve this issue. First, we applied a multisignal wavelet analysis on input multispectral data. Then, reconstructed signals from detail coefficients were used in conjunction with original input signals to do ICA. Finally, Fuzzy C-Means (FCM) clustering was performed on generated results for visual and quantitative analysis. Reproducibility and accuracy of the classification results from proposed method were evaluated by synthetic and clinical abnormal data. To ensure the positive effect of the new method in classification, we carried out a detailed comparative analysis of reproduced tissues with those from conventional ICA. Reproduced small abnormalities were observed to give good accuracy/Tanimoto Index values, 98.69%/0.89, in clinical analysis. Experimental results recommend MW-ICA as a promising method for improved brain tissue classification.

1. Introduction

Multispectral analysis of Magnetic Resonance Imaging (MRI) to access the relevant and complementary information from different sequences has been a widely discussed research topic for many years [1, 2]. MRI sequences like T1-weighted images (T1WI), T2-weighted images (T2WI), Proton Density Images (PDI), Fluid Attenuated Inversion Recovery (FLAIR), and so forth provide a huge repository of unique information on different tissues [2, 3]. For example, considerable contrast between Gray Matter (GM) and White Matter (WM) is available from T1WI. T2WI can give details of Cerebral Spinal Fluid (CSF) and abnormalities, whereas FLAIR images suppress CSF effects to give hyperintense lesions details. Simultaneous analysis of each sequence to collect the prominent pathological information is a tedious job for radiology experts. Computer-aided diagnosis using multispectral approach is helpful in this context to save time and to improve the accuracy and consistency of the clinical results [4]. But conventional algorithms used in normal data mining process are not efficient and robust to yield good results with expected clinical accuracy in multispectral analysis. Recent multispectral brain MRI analysis attempted to resolve this issue by improved feature extraction with statistical and mathematical concepts like probabilistic methods, fuzzy approaches, algebraic techniques, and so forth, [5–7].

A typical multispectral analysis system initializes with a collection of coregistered images as input data. Corresponding slices from each sequence forms each band in the multispectral suite as shown in Figure 1. Preprocessing steps like intensity inhomogeneity correction and noise removal [2] can be used to enhance the contrast and quality of the input images. Feature extraction and optimal selection of features are important in multispectral analysis, since accuracy and reliability of the classified results are highly affected by the selected feature sets [2]. Principal component analysis

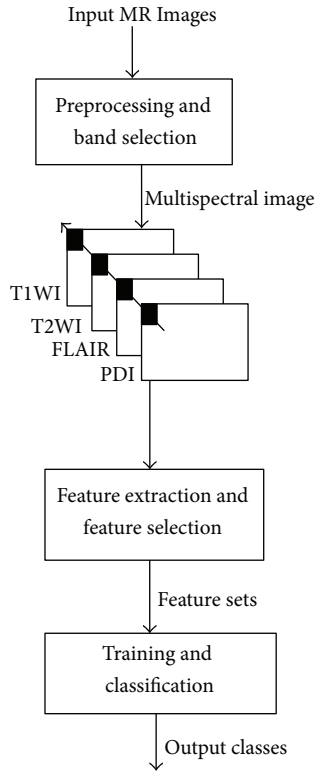

Figure 1: Typical multispectral analysis.

[8], wavelets [9], and Independent Component Analysis (ICA) [10] are the common feature extraction techniques in supervised and unsupervised multispectral classifications [8, 11]. Unsupervised classifications like k-means clustering [8], Fuzzy-C-Means (FCM) clustering [7], and self-organizing maps [8] were found to be yielding good results in automated segmentation and classification. Artificial Neural Networks (ANN) [2, 8], Support Vector Machines (SVM) [12], and ensemble methods have contributed a lot in clinically trained model preparation for pathological tissue analysis.

This work focuses on improvement in automated multispectral brain MRI classification through enhanced feature analysis. Recent brain MRI studies using ICA [13, 14] and its extensions like kernel ICA [13], overcomplete ICA [15], and so forth, have demonstrated ICA as a good feature extraction method for normal and abnormal tissue analysis. As a global transform, ICA gives more priority to global features, thereby losing important information on local brain matters in classification [16]. Dependency of the input MRI images also adversely affects the ICA based classification results. Local ICA [17] and Wavelet based ICA extensions [16, 18, 19] have been introduced as a solution for these shortcomings. However, the selection of decomposition levels and reconstruction errors on spatial wavelet analysis were found to influence the accuracy and reliability of the reproduced results in clinical analysis.

An improved source separation method, Multisignal Wavelet Independent Component Analysis (MW-ICA), is proposed in this work for efficient, automated brain tissue analysis from multispectral MRI. First, local characteristics from brain MRI images were extracted by multisignal wavelet analysis. High frequency components (detail coefficients) are mutually independent while low frequency components are weakly dependent [19]. So, detail coefficients were considered in this work for wavelet reconstruction to retain the mutually independent local details. Reconstructed signals were appended to original input signals to form an enhanced input signal set for ICA. FCM [7, 20] was then applied to results from ICA to do segmentation and classification. Visual and quantitative analyses, using synthetic and clinical data, were performed to evaluate the improvement in tissue classification by MW-ICA over conventional ICA. The variations in reproducibility of the new method for different wavelets were also considered in this study. Observed results demonstrated the reproducibility and efficiency of the proposed method in local and global brain matter classification.

The rest of the paper is organized as follows. Materials and methods are explained in Section 2. Experiments and results are presented in Section 3. Several aspects of our work are discussed in Section 4. Section 5 concludes the paper.

2. Materials and Methods

2.1. Input Data. Both synthetic and clinical images were considered in the evaluation of the proposed system. The synthetic MR images were collected from BrainWeb, Simulated Brain Database at the McConnell Brain Imaging Centre of the Montreal Neurological Institute (MNI), McGill University (http://www.bic.mni.mcgill.ca/brainweb/). We selected 20 slices (slices nos. 90–109) of abnormal data set containing multiple sclerosis (MS) details to form the multispectral suite. Axial T1-weighted images (T1WI), T2-weighted images (T2WI), and Proton Density Images (PDI) with parameter settings 1 mm slice thickness, intensity nonuniformity 20%, and noise level 0% were included in the set.

Axial T1WI, T2WI, and FLAIR images from 28 abnormal cases were considered for clinical image analysis. Three sample slices from each sequence showing traces of abnormal tissues were selected for each case, and total 28×3 multispectral image cubes were included in the analysis. The brain MR images were acquired by axial spin echo T1WI with repetition time (TR) = 1600 ms, echo time (TE) = 8.9 ms, and T2WI with TR/TE = 4000 ms/95 ms. FLAIR images have TR/TE = 6000 ms/94 ms, inversion time (TI) = 2026.5 ms. Additional parameters were slice gap 6.5 mm, thickness 5 mm, and the size 227×260 pixels. The ground truth tissues in clinical cases were collected from manually segmented and labeled images, under the supervision of an experienced radiologist.

2.2. Wavelet Analysis and Synthesis. In this work, images from each band in the multispectral cube were reshaped into a 1D signal, and a collection of those signals form MRI multisignal [19] were stored as a matrix organized rowwise (or columnwise). Wavelet transform of a signal is calculated by projection of the signal onto shifted and scaled version of a basic function [9]. In the case of higher dimensional signals, it can be done in spatial or spectral direction. Mallat's

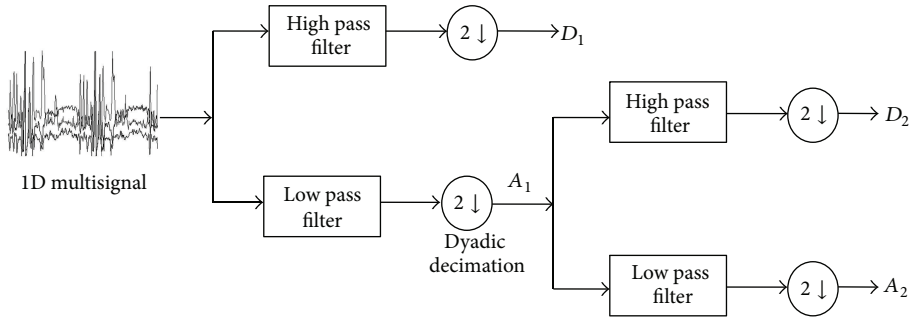

Figure 2: Multisignal wavelet analysis of multispectral data.

multiresolution algorithm [9] for 1-D signal was extended to multidimensional signals, as shown in Figure 2, to do multisignal wavelet analysis in this work.

A low pass filter and its corresponding high pass filter are simultaneously applied on input multisignal at each level "i" in its column direction (spectral domain). Spectra are decomposed into approximation coefficient A_i and detail coefficient D_i as shown in Figure 2. Irrelevant elements involved in the signals are eliminated by a dyadic decimation, which reduces the original resolution into half of its length. This procedure is recursively applied on approximation coefficients to give increasingly smoother versions of the original signals. Wavelet transforms can preserve low frequency and high frequency features through the explained multiresolution analysis. Studies show that high frequency subband signals are independent and low frequency subbands are weakly dependent [19]. In this work, only the local characteristics were required to preserve for classification. So independent high frequency subbands coefficients were considered in the multisignal wavelet reconstruction [9]. Reverse process of analysis is adopted in wavelet synthesis or reconstruction [19]. Wavelet decomposition involves filtering and downsampling, whereas wavelet reconstruction involves upsampling and filtering. The decomposed spectral data is lengthened by inserting zeros between every two samples of the signal (upsampling), and inverse filtering is applied.

Level of decomposition plays an important role in multiresolution analysis. Decomposing the spectra into too many, smaller levels will result in subband signals with more local details in high pass components [19], making approximation coefficients deviating a lot from original signals. So the decomposition level in this work was restricted to the greatest integer contained in $\log_2(d)$, where "d" is the dimension of multispectral cube.

2.3. Independent Component Analysis (ICA). ICA is a potential and promising approach in structural and functional MRI analysis [21]. The main concept of this technique lies in unmixing a set of independent sources according to their statistical independency from a linearly mixed input signal [10]. Let $\mathbf{x}$ be a column vector $\mathbf{x} = [x_1, x_2, \ldots, x_n]^T$, where x_i's are mixtures and $\mathbf{s} = [s_1, s_2, \ldots, s_m]^T$, be the sources. Using the vector-matrix notation, the above mixing model can be written as

$$\mathbf{x} = \mathbf{As}, \tag{1}$$

where "$\mathbf{A}$" is the matrix with elements a_{ij}. "$\mathbf{A}$" can be estimated and its inverse "$\mathbf{W}$" can be obtained to calculate the independent components (ICs) by using

$$\mathbf{s} = \mathbf{Wx}. \tag{2}$$

Theoretically, it tries to find a linear representation of nongaussian data by the projection of observed data on the rows of the matrix "$\mathbf{W}$" (basis vectors) in which the transformed components are statistically independent, or as independent as possible [10]. The method for estimation of "$\mathbf{W}$" is based on contrast (or objective) functions that are calculated from some statistical properties of the data. The minimization or maximization of these functions and the relative adaptive change of the weights allow the final estimation of "$\mathbf{W}$". Several objective functions have been proposed for the estimation of the projection matrix "$\mathbf{W}$." These functions are based on likelihood, entropy, mutual information, or more frequently their approximations [10, 22].

In this work, "$\mathbf{x}$" is an L-dimensional pixel vector in the input image cube which is linearly mixed by a set of "m" statistically independent tissues or tumour information, $s_1, s_2, \ldots, s_m$, by means of a "$L \times m$" mixing matrix "$\mathbf{A}$" as in (1). FastICA algorithm [10] is applied on "$\mathbf{x}$" to extract "m" unknown signal sources (tissues and lesions) from the image cube. It is considered as an over-complete problem since $L < m$; that is, there are fewer images than the sources to be unmixed. According to linear system of equations, there exist many solutions to solve (1) and there is no way to select best ICs to perform classification [21]. If the number of signal sources is greater than the number of ICs, more than one signal characteristics are accommodated in the same IC. Enhancing the input matrix by reconstructed signals from detail coefficients in MW-ICA solves this issue to some extent.

2.4. Fuzzy C-Means Clustering (FCM). It is a data clustering technique introduced by Bezdec in 1981 [20], where each data

point belongs to a cluster to some degree, that is, specified by a fuzzy membership grade [23]. Let $\mathbf{X} = (x_1, x_2, \ldots, x_N)$ denotes an image with N pixels to be partitioned into c clusters, where x_i represents multispectral (features) data and "c" is the number of clusters with $2 \leq c < n$. The standard FCM objective function for partitioning a dataset $\{x_k\}_{k=1}^{N}$ into "c" clusters is given by [24]

$$J_m = \sum_{i=1}^{c} \sum_{k=1}^{N} U_{ik}^{m} \|x_k - v_i\|^2, \tag{3}$$

where $\{v_i\}_{i=1}^{c}$ are the centers of the clusters and the array $\{U_{ik}\}$, $i = 1, \ldots, c$, $k = 1, \ldots, N$ is a partition matrix such that

$$U \in \left\{ U_{ik} \in [0,1] \mid \sum_{i=1}^{c} U_{ik} = 1, \forall k, 0 < \sum_{k=1}^{N} U_{ik} < N, \forall i \right\}. \tag{4}$$

The parameter "m" is a weighting exponent on each fuzzy membership, and it determines fuzziness amount of the resulting classification. Gray level values are the most commonly used feature in image processing. So FCM objective function J_m is minimized when high membership values are assigned to pixels whose intensities are close to the centroid of its particular class, and low membership values are assigned when the point is far from the centroid [24]. In the FCM algorithm, the probability that a pixel belongs to a specific cluster depends only on the distance between the pixel and each individual cluster center in the feature domain. Algorithm starts with an initial guess for each cluster centre, and it converges to a solution for v_i representing the local minimum or a saddle point of the objective function J_m. A detailed explanation of FCM theorem and algorithm is available in [25].

2.5. Proposed Algorithm, MW-ICA, for Classification. Wavelet decomposition of the spectra and ICA are the core concepts used in this algorithm. Major steps involved in this method are depicted in Figure 3. Co-registered corresponding images from different MRI sequences are used to form a multispectral suite. Each pixel vector represents the spectral signature of the area specified by that pixel. Consider input multispectral image as a collection of spectral signatures, represented by ray passing through the pixel vector as shown in Figure 3. Apply 1-D multisignal wavelet decomposition to these signals to divide the spectral domain into low frequency and high frequency components as described in Section 2.2. To retain the importance of the small features, only the detail coefficients are considered in wavelet reconstruction.

The reconstructed signals are combined with input multisignals, and ICA using FASTICA [10] algorithm is applied on newly formed dataset. FCM clustering algorithm is applied on each generated IC to classify the brain matters automatically. The classified results are labeled by an experienced radiologist for analysis of normal and abnormal brain tissues. The proposed algorithm can be summarized as follows.

Input. MRI Images I_1, I_2, I_3, I_4, and so forth, representing co-registered T1WI, T2WI, PDI, FLAIR, and so forth.

Step 1. Create p-dimensional multispectral image cube $M = [I_1, I_2, I_3, I_4, \ldots, I_p]$ from "p" input images.

Step 2. Reshape each image into its 1-D form and generate a p-dimensional multisignal $\mathbf{X}$.

Step 3. Apply multisignal wavelet analysis on $\mathbf{X}$ to decompose the signals into approximation coefficients and detail coefficients.

Step 4. Apply multisignal wavelet reconstruction algorithm on detail coefficients to obtain reconstructed signal $\mathbf{X}^*$.

Step 5. Expand $\mathbf{X}$ by appending $\mathbf{X}^*$ and form new input multisignal $\mathbf{X}_{\text{new}}$ of dimension "n" $\leq 2p$.

Step 6. Apply ICA on $\mathbf{X}_{\text{new}}$ to generate "n" unmixed components.

Step 7. Reshape each component to corresponding 2D form and apply FCM algorithm.

Step 8. Segmented results from Step 7 are classified into different brain tissues for further analysis.

2.6. Performance Measures. Tanimoto Index, sensitivity, specificity, accuracy, False Positive Rate (FPR), and error rate were the measures used in quantitative analysis in this study. Tanimoto Index, the most commonly used measurement in medical imaging [14], can be measured by comparing the reproduced tissues with ground truth using the formula

$$T = \frac{|A \cap B|}{|A \cup B|}, \tag{5}$$

where A and B are two datasets involved in the classification comparison. Similarity checking of brain tissues CSF, GM, WM, and tumor with corresponding ground truth was performed in this work using (5). Sensitivity, specificity, accuracy, error rate, and False Positive Rate (FPR) were calculated from confusion matrix [26] as follows:

$$\begin{aligned}
&\text{Sensitivity} = (\text{TP}/(\text{TP} + \text{FN})) * 100\%,\\
&\text{Specificity} = (\text{TN}/(\text{TN} + \text{FP})) * 100\%,\\
&\text{Accuracy} = ((\text{TP} + \text{TN})/(\text{TP} + \text{TN} + \text{FP} + \text{FN})) * 100\%,\\
&\text{FPR} = \text{FP}/(\text{TN} + \text{FP}) * 100\%,\\
&\text{Error Rate} = (1 - \text{Accuracy}) * 100\%.
\end{aligned}$$

True Positive (TP) represents the number of correctly identified positive pixels (for example, tumor), whereas False Positive (FP) gives the count of negative pixels (for example, normal tissues) incorrectly identified as positive (tumor). Correctly identified negative pixels are measured as True

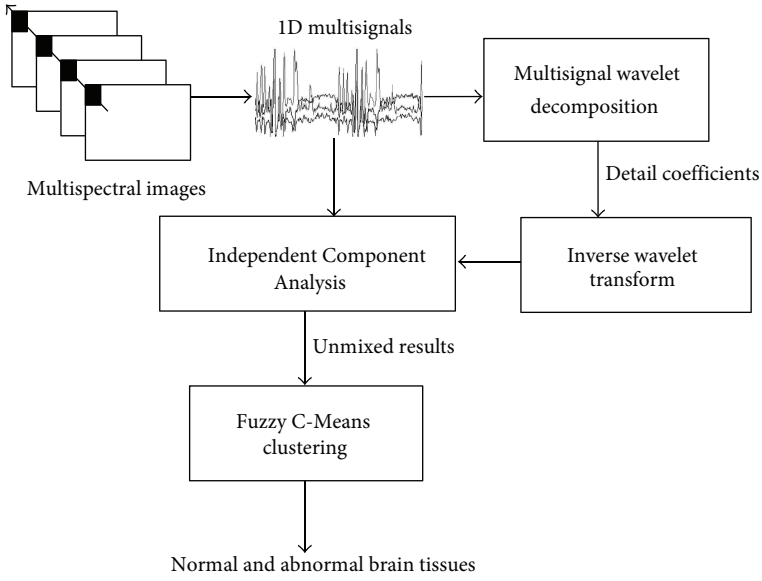

Figure 3: Proposed MW-ICA based classification.

Negative (TN), and positive pixels incorrectly identified as negative tissues are counted as False Negative (FN). Sensitivity represents the proportion of actual positives (here tissues like GM, WM, etc.) correctly classified and specificity is the proportion of negatives (here other tissues and background) correctly identified.

We used an additional method, Bland-Altman analysis [27], to evaluate the agreement between measures from two methods. In the Bland-Altman plots, difference between two measurements (the bias) is plotted against the average of those measurements. In this work, the reproduced lesion volumes by ICA and MW-ICA were quantitatively compared with lesion volumes by the groundtruth using this method.

3. Experiments and Results

The complete system for algorithm implementation and evaluation was done in Matlab 7 running on Windows 7. The proposed method was evaluated by both synthetic and clinical MRI images described in Section 2.1. Co-registered images were selected for wavelet decomposition and ICA. No image registration was required in the case of synthetic images, but Matlab based simple resizing and rotation was applied on clinical images to generate co-registered data. Multisignal 1-D wavelet analysis was applied on input signals using Matlab Wavelet Toolbox. Wavelets from Daubechies [28] family were selected for detailed performance variation study for different wavelets. FCM method provided in Fuzzy Logic Toolbox was applied on generated ICs to do automatic segmentation. Feature extraction and classification by FCM were the main steps in this study. Quantitative and qualitative analyses were performed using reproduced results from synthetic and real data. These experiments were repeated for conventional ICA based FCM also. After that, we conducted a comparative study of two methods in the same environment. The observed results are presented, and they are discussed in the following sections.

3.1. Synthetic Image Analysis. Multiple sclerosis (MS) data obtained from the BrainWeb Simulated Brain Database was included in synthetic MR image analysis. 20 multispectral image sets were formed from axial T1-weighted images (T1WI), T2-weighted images (T2WI), and Proton Density Images (PDI) with specifications described in Section 2.1. Figure 4(a) shows images of slice no. 105 for different sequences. T1WI shows WM and GM components, T2WI gives details of CSF and White Matter lesions (WML), and PD images show abnormal features. Reconstructed images from multisignal wavelet analysis are given in Figure 4(b). Results from MW-ICA and ICA are shown in Figures 4(c) and 4(d), respectively. As described in Steps 5 and 6 of the proposed method, total six ICs were generated from MW-ICA using Db12 wavelet. Relevant four of them are shown in Figure 4(c). Details of the brain features provided by MW-ICA (Figure 4(c)) were found to be very specific in providing brain matter details from each component, showing CSF, WM, WML, and GM features clearly in 1st, 2nd, 3rd, and 4th ICs, respectively. However it was observed from conventional ICA results (Figure 4(d)) that features of CSF and WML were accumulated in 1st IC, whereas proposed method clustered CSF and WML into different classes. Presence of WML locations in WM (Figure 4(d) 3rd IC) was not so clear in ICA results.

We analyzed the effect of these feature analysis methods in FCM clustering, for a given degree of membership 0.6, and reproduced tissues are presented in Figure 5. Figure 5(a) shows MW-ICA based FCM results, and ICA based FCM results are shown in Figure 5(b). Each column represents a particular brain tissue in the order of CSF, GM, WM, and WML from left to right. The best results by proposed method

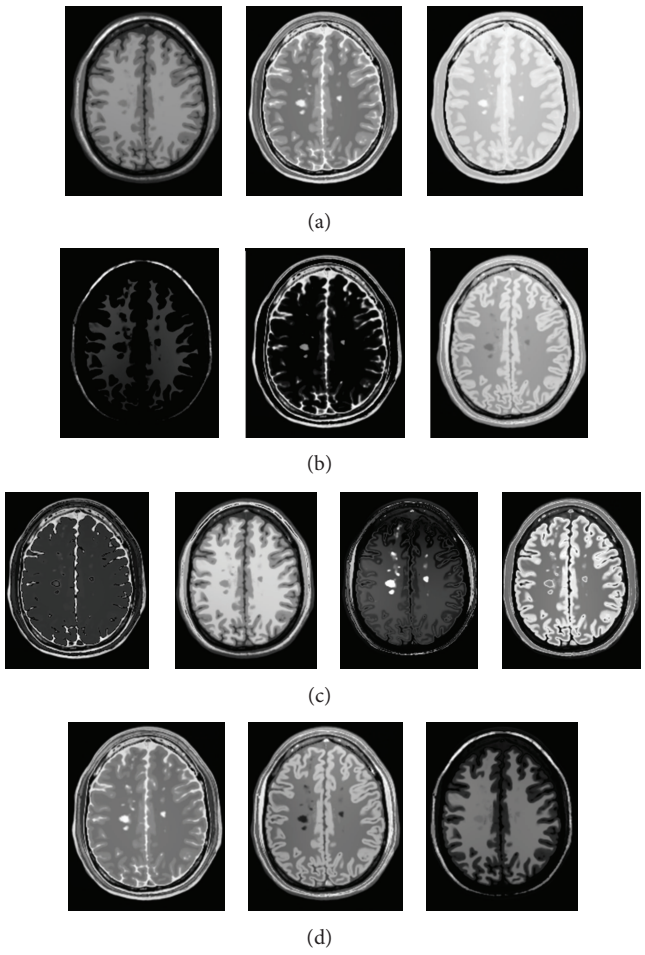

Figure 4: ICA and MW-ICA results from synthetic image analysis. (a) Synthetic Images T1WI, T2WI and PDI from left to right. (b) Reconstructed images from detail coefficients. (c) Independent components from proposed method. (d) Conventional ICA results.

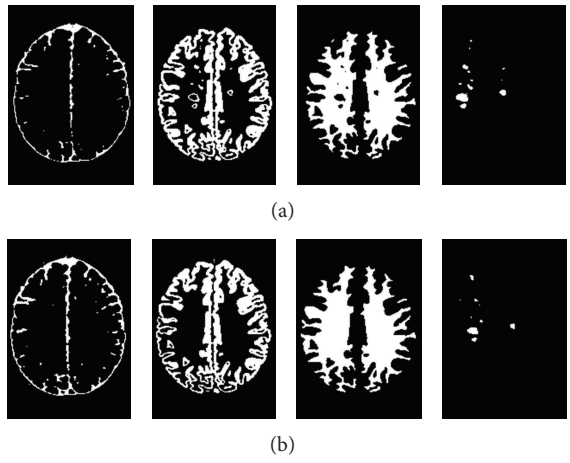

Figure 5: FCM Classification results in the order of CSF, GM, WM and WML from left to right. (a). Results from MW-ICA (b). Results from ICA.

were observed for small lesions and WM. The presence of abnormality in WM is clearly visible in Figure 5(a) 3rd column. MW-ICA based classification results gave more information on lesion details (Figure 5(a)) than those from ICA based processing (Figure 5(b)). GM tissues (2nd column) were found to be more specific in MW-ICA results, but traces of negative pixels were also found in the classified results.

To evaluate the improvement in MW-ICA based classification, a detailed quantitative analysis was performed with 15 synthetic multispectral sets. Average sensitivity, specificity, accuracy, False Positive Rate (FPR), error rate (all in %), and Tanimoto Index (TI) values were measured for FCM classifications based on ICA and MW-ICA for membership degree 0.8. Observed results are summarized in Table 1. Experimental reports demonstrated the efficiency of the proposed method by yielding comparatively better results for all tissues. A drastic increase in Tanimoto Index and sensitivity observed in the case of WM lesions, showing 0.93 against 0.82 for TI, and sensitivity increased from 85.88% to 93.23%. From visual and quantitative results, it was observed that MW-ICA could improve the reproducibility of local features like small lesions in classification. To confirm the efficiency and consistency of the proposed algorithm for different wavelets, db2, db4, db8, db12, db16, db24 and db32 were also considered in quantitative analysis. TI values and error rate observed for GM, WM, and WML were plotted as shown in Figures 6(a) and 6(b), respectively. X-axis shows Daubechies wavelets of different orders "N" [28]. From Figure 6(a), Db4 is the best for WM, and Db12 shows the next best value. For GM and lesion extraction, Db12 exceeds Db4. Difference in error rate on variation of wavelet orders is available from Figure 6(b). For lesions, least error rate value was observed for Db12. However, Db4 showed the best values for GM and WM.

To interpret the performance improvement by MW-ICA over ICA statistically, Bland-Altman analysis was performed on 20 synthetic multispectral sets. The differences between lesion volumes (in mL) estimated from ICA based results and the groundtruth were first plotted against the averages of both measures (Figure 7(a)). The agreement between MW-ICA and the groundtruth was plotted as shown in Figure 7(b). The mean difference (bias or d), standard deviation (SD) of the differences, and 95% limits of agreement (±1.96 SD) were also calculated. Using ICA, d was 0.24 mL with 95% limits of agreement, −0.11 mL to 0.58 mL (Figure 7(a)), whereas the points were distributed closer to zero for MW-ICA. Mean bias was observed as 0.05 mL with 95% limits of agreement, −0.05 mL to 0.16 mL (Figure 7(b)).

Visual and quantitative analyses by synthetic images supported the positive impact of MW-ICA in brain tissue classification with relatively good normal and abnormal reproduced tissues. In order to evaluate the efficiency of the proposed method in clinical analysis, abnormal data from 28 patients were selected, and experimental results are discussed in the next section.

3.2. Clinical Image Analysis. The same sets of experiments explained in previous section were repeated for abnormal

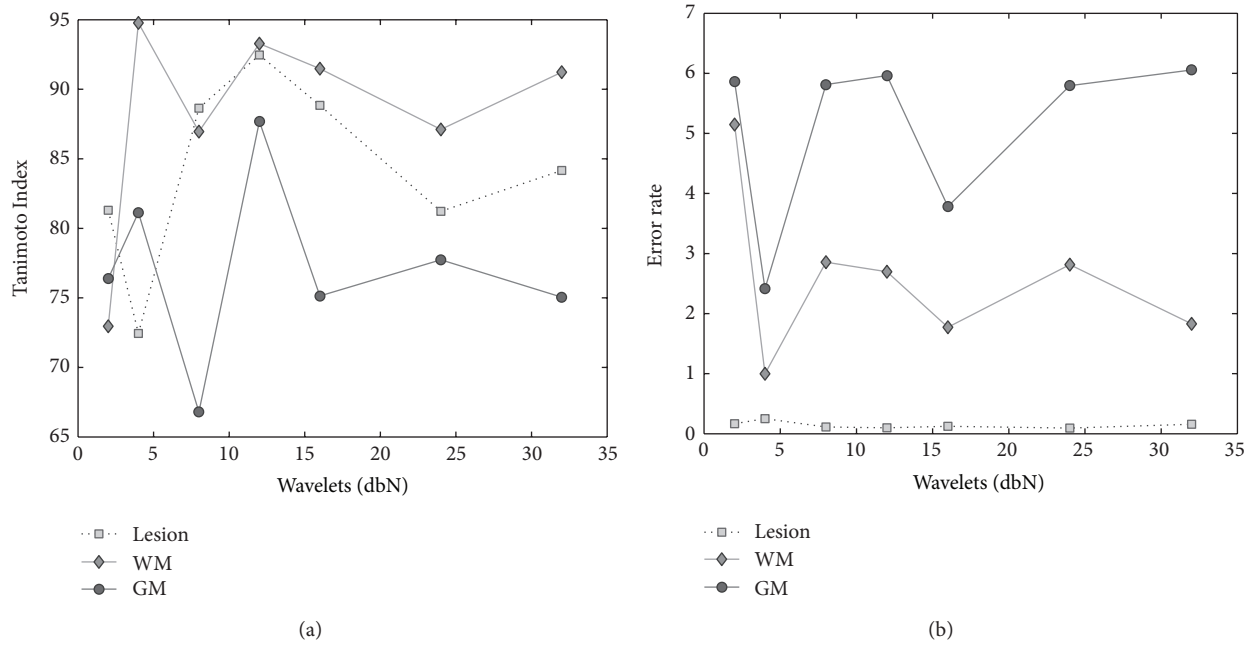

Figure 6: Performance measure variations for Daubechies wavelets with different orders "N". (a) Tanimoto Index (b) Error rate.

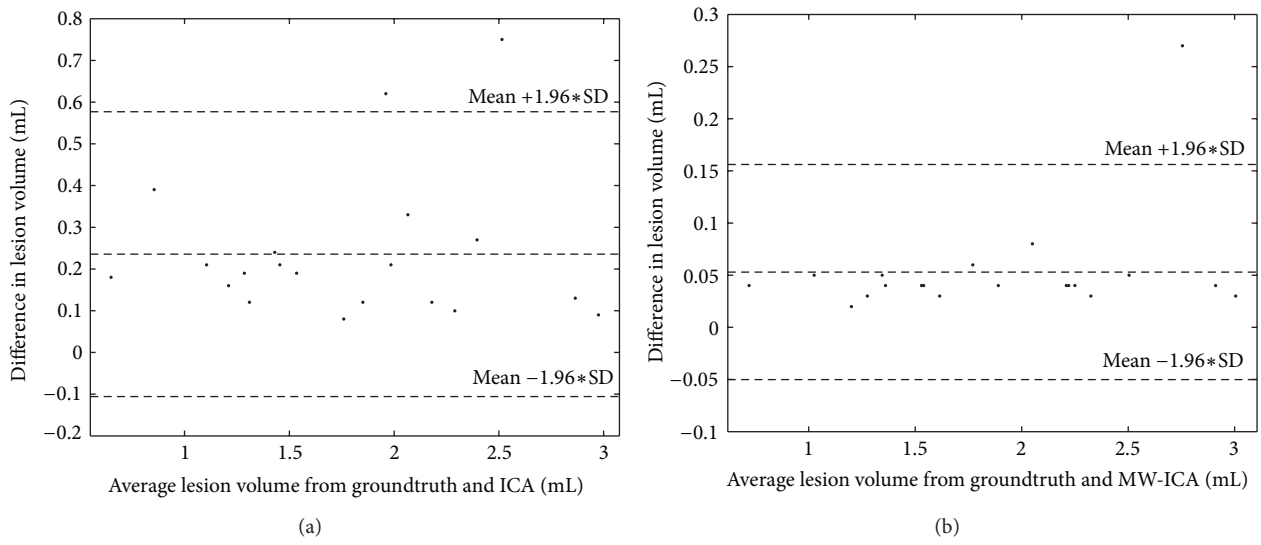

Figure 7: Bland-Altman plots showing the statistical agreement between lesion volumes obtained from groundtruth and (a) ICA based classification. (b) MW-ICA based classification. The dotted lines represent the mean and 95% limits of agreement.

data to verify the clinical performance of the proposed method. Three bands in multispectral image were formed from axial T1WI, T2WI, and FLAIR images with parameters and specification as discussed in Section 2.1. Total 28 × 3 multispectral sets were resulted by selecting three different abnormal slices for each case. Figure 8(a) shows sample input images, T1WI, T2WI, and FLAIR, selected for visual analysis. WM details are available from T1WI; T2WI shows CSF and abnormal points. FLAIR images give information on abnormal tissues. No detailed information on GM was available from these images. ICA based FCM was first applied on this dataset. Classified results with degree of membership 0.9 are shown in Figure 8(b). We repeated MW-ICA based FCM on the same dataset using Db12 wavelet. Reproduced tissues, CSF, WM, and abnormality are shown in Figure 8(c) from left to right. Column wise comparison of Figures 8(b) and 8(c) can give a detailed picture of the improvement in tissue classification by proposed method. CSF details from 1st column of Figure 8(b) is found to be more than that from Figure 8(c). But ICA results in Figure 8(b) failed to give specific details of abnormality in the 2nd and 3rd columns. Visual results demonstrated the efficiency of MW-ICA in

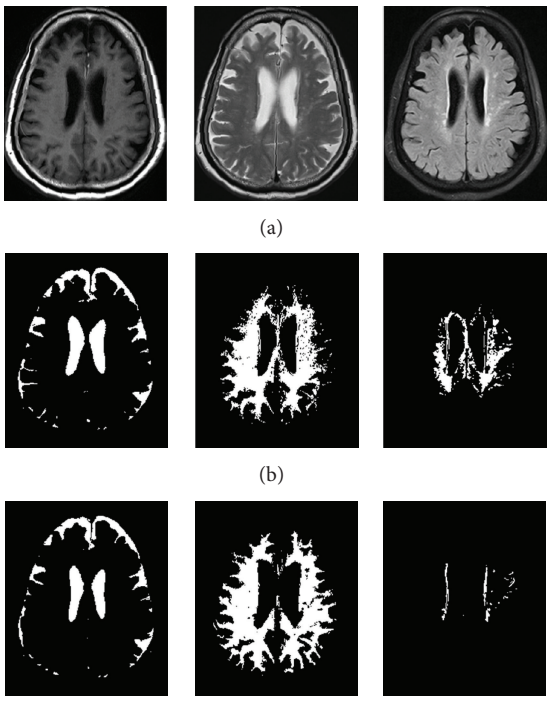

Figure 8: FCM Classification results in the order of CSF, WM and WML from left to right. (a) Clinical input images, T1WI, T2WI and FLAIR from left to right. (b) ICA based results. (c) MW-ICA based results.

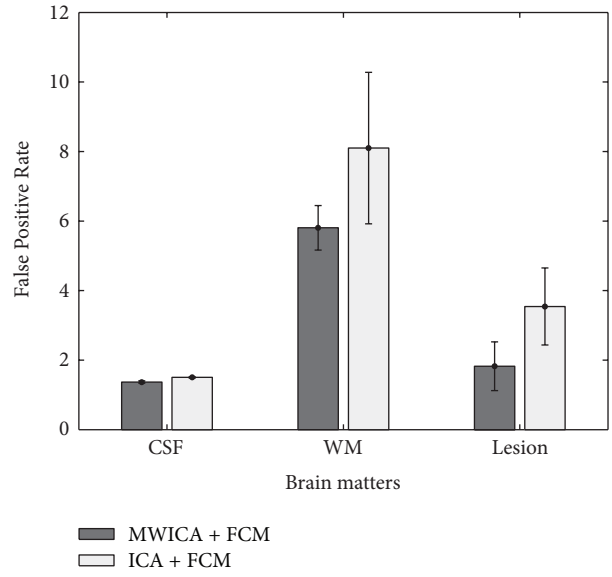

Figure 9: FPR comparison of segmented tissues using MW-ICA and ICA.

small feature analysis with highly specific WM and abnormal reproduced tissues. Results from Figure 8(c) show that abnormalities extracted by proposed method are very similar to those available from FLAIR image. Its presence in WM is also located correctly by proposed method. To ensure the efficiency of the new method in clinical analysis, an elaborate study was performed with quantitative measurements like the sensitivity, specificity, accuracy, error rate (all in %), and Tanimoto Index values. Average measures from classification of 84 multispectral slice sets, along with standard deviation values (std.), are summarized in Table 2.

Table 2 results describe MW-ICA as a better approach compared to ICA in brain tissue analysis. Proposed method gave very good results for all tissue except CSF. ICA performed better in classification of CSF with average TI value 0.66 ± 0.09 against 0.61 ± 0.01, but it shows large standard deviations for sensitivity and Tanimoto measures. In the case of small abnormality analysis, Tanimoto value improved from 0.792 ± 0.12 to 0.90 ± 0.07. Almost the same amount of improvement was observed in the case of WM analysis also. Consistency of the new method was confirmed by the reduction in standard deviations observed for almost all measures.

Average results from three multispectral slice sets of a single patient, measured by ICA based classification and MW-ICA based analysis, were used to study the variation in False Positive Rate. Estimated results from 28 patients with standard deviations are shown as error bars in Figure 9 for CSF, WM, and abnormality. CSF classification from MW-ICA and ICA showed almost the same results. However, in the case of WM and abnormality analysis, comparatively lower values were observed for MW-ICA based analysis. The significant reduction in FPR observed for MW-ICA based classification, in the case of abnormal tissues, is a promising result in clinical analysis.

4. Discussion

In this work, we have proposed a new method, Multisignal Wavelet Independent Component Analysis (MW-ICA), for improved feature extraction and brain tissue classification from multispectral MRI. ICA is a good preprocessing step in multispectral classification. It separates the mixed input signals into statistically independent components (ICs), from which an improved brain tissue classification can be performed in MRI analysis [14]. However, it ignores small details while processing massive amount of information. As an attempt to resolve this issue, high frequency components (detail coefficients) from multisignal wavelet analysis were considered in this work in conjunction with input multisignals. The algorithm was validated by both synthetic and real images. It was implemented as an automated technique, in which the ICs were derived automatically from co-registered images. Parameters like wavelet type and degree of membership were set as fixed in the initial settings. The new method succeeded in unmixing each brain tissue into separate ICs, from which a reliable automatic segmentation using FCM was performed without any indexing. In comparison with ICs from widely used ICA method (Figure 4(d)), MW-ICA provides more tissue specific components (Figure 4(c)). Lesion detection from ICA results was not very easy, since CSF and lesion details were accumulated in first component

Table 1: Quantitative analysis of synthetic images.

	Feature analysis	Sensitivity	FPR	Specificity	Accuracy	TI
CSF	ICA	84.18	0.76	99.24	97.18	0.75
	MW-ICA	88.19	0.39	99.61	98.49	0.78
WM	ICA	99.53	1.99	98.01	98.31	0.90
	MW-ICA	99.60	2.08	96.92	97.44	0.93
WML	ICA	85.88	0.07	99.91	99.61	0.82
	MW-ICA	93.23	0.09	99.91	99.80	0.93
GM	ICA	95.28	5.13	94.87	94.92	0.82
	MW-ICA	98.90	2.98	97.03	96.94	0.88

Table 2: Quantitative analysis of clinical images.

	Feature analysis	Sensitivity (±std.)	Specificity (±std.)	Accuracy (±std.)	TI (±std.)
CSF	ICA	66.28 (9.34)	99.99 (0.02)	95.21 (2.42)	0.66 (0.09)
	MW-ICA	67.35 (5.47)	98.52 (1.40)	94.76 (2.81)	0.61 (0.01)
WM	ICA	85.50 (8.20)	94.08 (4.36)	92.37 (2.26)	0.70 (0.05)
	MW-ICA	88.95 (7.14)	94.83 (1.28)	93.60 (2.18)	0.81 (0.01)
WML	ICA	84.90 (5.02)	97.57 (2.22)	97.31 (2.18)	0.72 (0.12)
	MW-ICA	91.99 (3.88)	98.88 (1.40)	98.69 (1.38)	0.90 (0.07)

(Figure 4(d)). ICA results failed to locate the presence of lesions in WM (Figure 4(d) last column) because of background dominating effects from global features.

The reproduced tissues from proposed method were evaluated qualitatively and quantitatively against groundtruth images and ICA based results. Classified brain tissues from synthetic images, especially WM and WML, were found to be yielding more information with improved quality (Figure 5(a)) compared to ICA based results (Figure 5(b)). It is further emphasized by the visual results from clinical case also (Figure 7). Performance measures like TI, sensitivity, specificity, accuracy, and so forth, discussed in Section 2.6, demonstrated the potential of MW-ICA based FCM in classification of global and local features with relatively better values compared to ICA based classification (Table 1). Tanimoto Index/sensitivity values, 0.93/93.23%, observed against 0.82/85.88%, for synthetic case WM lesion analysis confirmed the improvement in small object detection by MW-ICA. Improved sensitivity and accuracy values observed for all tissues demonstrated the efficiency and robustness of the new algorithm in clinical trials (Table 2). Increased average TI value from 0.72 to 0.90 and reduced FPR (Figure 9) support the effectiveness of the method in small abnormality analysis. Considerable reduction in standard deviation (Table 2 and Figure 9) implies the consistency of MW-ICA based classification in clinical analysis. Statistical interpretation of agreement between estimated synthetic lesion volumes by groundtruth and classifications using MW-ICA (and ICA) was performed with Bland-Altman analysis. A closer agreement with segmented brain volumes, from groundtruth and MW-ICA, supports the new method as a better approach compared to ICA. Bias was contained well within the two standard deviations except for one sample (Figure 7(b)). Improvement in MW-ICA over ICA was further confirmed by the reduced mean bias (which is closer to zero) and shortened limits of agreement.

Variation in quantitative measures, TI, and error rate for different wavelets implied that wavelet selection has an important role in quality of the results (Figure 6). Considering the cost of feature extraction, MW-ICA was observed to take more time. We measured 0.45 seconds for ICA, and 1.43 seconds for MW-ICA in a typical clinical imaging analysis, on a Windows 7 PC with Pentium Dual CPU of 2.0 GHz/2 GB RAM. It can be varied on different values of parameters like wavelet type, degree of decomposition, number of bands in input signals, and so forth which is to be explored in future works. The common MR image artefacts like gaussian noise, illumination effects, and so forth, were not considered in this work.

Experimental results support MW-ICA as a promising approach in classification of brain matters, especially in the case of small abnormalities. Technically, novelty of the algorithm lies in exploiting the characteristics of the wavelets in extracting the local features and combining the results with input multisignal for improved segmentation and classification. Experimental results demonstrated it in clinical analysis of brain matters, especially in locating small lesions and their effect on other brain tissues. A detailed analysis of the proposed method using optimal parameter selection and supervised methods is under consideration as a future work.

5. Conclusion

We presented a new Multisignal Wavelet ICA (MW-ICA) based classification to improve the performance of automated multispectral MRI analysis. FCM clustering was used to investigate and evaluate the positive effect of the method in

brain tissue analysis. Experimental results using synthetic and clinical data confirmed the efficiency and reproducibility of the proposed method in small abnormality analysis. Comparative analysis with ICA based classifications recommends that MW-ICA can be a good choice for automatic brain tissue classification in clinical analysis. Supervised classification using MW-ICA in noisy environments is under consideration as a future work.

Acknowledgment

The authors sincerely thank the Institute of Radiology and Imaging Sciences (IRIS) Pvt. Ltd., Kochi, for supporting them with the required medical guidance in this work.

References

[1] M. W. Vannier, R. L. Butterfield, and D. Jordan, "Multispectral analysis of magnetic resonance images," *Radiology*, vol. 154, no. 1, pp. 221–224, 1985.

[2] L. P. Clarke, R. P. Velthuizen, M. A. Camacho et al., "MRI segmentation: methods and applications," *Magnetic Resonance Imaging*, vol. 13, no. 3, pp. 343–368, 1995.

[3] Y. Kvinnsland, N. Brekke, T. M. Taxt, and R. Grüner, "Multispectral analysis of multimodal images," *Acta Oncologica*, vol. 48, no. 2, pp. 277–284, 2009.

[4] H. Arimura, T. Magome, Y. Yamashita, and D. Yamamoto, "Computer-aided diagnosis systems for brain diseases in magnetic resonance images," *Algorithms*, vol. 2, no. 3, pp. 925–952, 2009.

[5] C. Valdés Hernández Mdel, P. J. Gallacher, M. E. Bastin et al., "Automatic segmentation of brain white matter and white matter lesions in normal aging: comparison of five multispectral techniques," *Magnetic Resonance Imaging*, vol. 30, no. 2, pp. 222–229, 2012.

[6] A. Akselrod-Ballin, M. Galun, J. M. Gomori et al., "Automatic segmentation and classification of multiple sclerosis in multichannel MRI," *IEEE Transactions on Bio-Medical Engineering*, vol. 56, no. 10, pp. 2461–2469, 2009.

[7] R. He, S. Datta, B. R. Sajja, and P. A. Narayana, "Generalized fuzzy clustering for segmentation of multi-spectral magnetic resonance images," *Computerized Medical Imaging and Graphics*, vol. 32, no. 5, pp. 353–366, 2008.

[8] C. M. Bishop, *Pattern Recognition and Machine Learning*, Springer, 2006.

[9] S. Mallat, *A Wavelet Tour of Signal Processing*, The Sparse Way Academic Press, 3rd edition, 2008.

[10] A. Hyvarinen, J. Karhunen, and E. Oja, *Independent Component Analysis*, John Wiley & Sons, New York, NY, USA, 2001.

[11] S. Ozer, D. L. Langer, X. Liu et al., "Supervised and unsupervised methods for prostate cancer segmentation with multispectral MRI," *Medical Physics*, vol. 37, no. 4, pp. 1873–1883, 2010.

[12] V. N. Vapnik, *Statistical Learning Theory*, John Wiley & Sons, New York, NY, USA, 1998.

[13] T. Tateyama, Z. Nakao, and Y. W. Chen, "Classification of brain matters in MRI by Kernel Independent Component Analysis," in *Proceedings of the 4th International Conference on Intelligent Information Hiding and Multiedia Signal Processing (IIH-MSP '08)*, pp. 713–716, August 2008.

[14] J. W. Chai, C. C. C. Chen, C. M. Chiang et al., "Quantitative analysis in clinical applications of brain MRI using independent component analysis coupled with support vector machine," *Journal of Magnetic Resonance Imaging*, vol. 32, no. 1, pp. 24–34, 2010.

[15] Y. C. Ouyang, H. M. Chen, J. W. Chai et al., "Band expansion-based over-complete independent component analysis for multispectral processing of magnetic resonance images," *IEEE Transactions on Biomedical Engineering*, vol. 55, no. 6, pp. 1666–1677, 2008.

[16] H. Han and X. L. Li, "Multi-resolution independent component analysis for high-performance tumor classification and biomarker discovery," *BMC Bioinformatics*, vol. 12, no. 1, article S7, 2011.

[17] J. Karhunen, S. Malaroiu, and M. Ilmoniemi, "Local independent component analysis using clustering," *International Journal of Neural Systems*, vol. 10, no. 6, pp. 439–451, 2000.

[18] J. Walters-Williams and Y. Li, "Performance comparison of known ICA algorithms to a wavelet-ICA merger," *Signal Processing*, vol. 5, no. 3, pp. 80–92, 2011.

[19] S. Kaewpijit, J. L. Moigne, and T. El-Ghazawi, "Automatic reduction of hyperspectral imagery using wavelet spectral analysis," *IEEE Transactions on Geoscience and Remote Sensing*, vol. 41, no. 4, pp. 863–871, 2003.

[20] J. C. Bezdec, *Pattern Recognition with Fuzzy Objective Function Algorithms*, Plenum Press, New York, NY, USA, 1981.

[21] Y. Ouyang, H. Chen, J. Chai et al., "Independent component analysis for magnetic resonance image analysis," *EURASIP Journal on Advances in Signal Processing*, vol. 2008, Article ID 780656, 2008.

[22] J. F. Cardoso, "Infomax and maximum likelihood for blind source separation," *IEEE Signal Processing Letters*, vol. 4, no. 4, pp. 112–114, 1997.

[23] X. F. Yang and B. W. Fei, "A multiscale and multiblock fuzzy C-means classification method for brain MR images," *Medical Physics*, vol. 38, no. 6, pp. 2879–2891, 2011.

[24] D. Zhang and C. Chen, "A novel kernelized fuzzy c-means algorithm with application in medical image segmentation," *Artificial Intelligence in Medicine*, vol. 32, pp. 37–50, 2004.

[25] A. O. Boudraa, S. M. R. Dehak, Y. M. Zhu, C. Pachai, Y. G. Bao, and J. Grimaud, "Automated segmentation of multiple sclerosis lesions in multispectral MR imaging using fuzzy clustering," *Computers in Biology and Medicine*, vol. 30, no. 1, pp. 23–40, 2000.

[26] J. Han and M. Kamber, *Data Mining: Concepts and Techniques*, Morgan Kaufmann Publisher, San Fransisco, Calif, USA, 2nd edition, 2006.

[27] J. M. Bland and D. G. Altman, "Statistical methods for assessing agreement between two methods of clinical measurement," *Lancet*, vol. 1, pp. 307–310, 1986.

[28] I. Daubechies, *Ten Lectures on Wavelets*, SIAM, Philadelphia, Pa, USA, 1992.